Indian Journal of Pure & Applied Physics
Vol. 63, July 2025, pp. 571-583
DOI: 10.56042/ijpap.v63i7.9196

XAFS Study of Mixed Ligand Ethylenediamine Copper Complexes Having Distorted Octahedral Coordination Geometry

Monica Bairagi[a,*], Vijay Kumar Hinge[b], Nishchhal Yadav[a], Santosh Kumar Joshi[c], Basant Deo Shrivastava[a], Shambhu Nath Jha[d] & Dibyendu Bhattacharya[e]

[a]School of Studies in Physics, Vikram University, Ujjain 456 010, India

[b]Ujjain Engineering College, Ujjain 456 010, India

[c]Physics Department, Government PG Arts & Science College, Ratlam 457 001, India

[d]Beamline Development and Application Section BARC, Mumbai and BARC Beamline Section, RRCAT, Indore, India

[e]Atomic & Molecular Physics Division, Bhabha Atomic Research Centre, Mumbai 400 085, India

Received: 29 February 2025; accepted: 5 June 2025

X-ray absorption fine structure (XAFS) at the Cu K-edge in copper complexes, viz., $Cu(en)_2Br_2.H_2O$, $Cu(en)_2Cl_2.H_2O$, $Cu(en)_2(ClO_4)_2$, $Cu(en)_2SO_4$,where en= ethylene-diamine, have been investigated using synchrotron radiation. For the analysis of EXAFS, theoretical models have been generated for each complex using their available crystal structure data. The theoretical models have been fitted to the respective experimental data by two methods. In the first method, the coordination number N has been varied and amplitude reduction factorS_0^2 has been fixed. In the second method, N has been fixed and S_0^2 has been varied.The results obtained by the two methods have been compared with each other.Ab-initio XANES calculations have been performed to obtain simulated XANES spectra as well as p-DOS and d-DOS for the absorbing Cu metal center. The XANES calculations reproduce well the absorption edge in the experimental XANES spectra. The splitting of Cu K-edge into two edges K_1 and K_2 has been correlated with the p-DOS. The separation of the K_1 and K_2 peaks in the derivative experimental spectra agree well with the derivative simulated spectra. The occurrence of pre-edge has been correlated with d-DOS.

Keywords: Copper complexes of ethylenediamine, Extended X-ray absorption fine structure, X-ray absorption near edge structure, Ab initio calculations, Density of states

1 Introduction

Ethylenediamine (en) is a basic amine which is commonly used as building block in chemical synthesis. It is one of the most widely used nitrogen containing ligands in coordination chemistry. The ligand can form staggered trans and gauche conformations about the C-C bond. In the condensed phases, en complexes of metal ions are mostly in the chelating mode[1]. The hetero ligand copper complexes with en and various inorganic and organic ligands are attractive due to ease of synthesis, catalytic activity, and practical applications in industry, agriculture, microelectronics, and medicine. The use of polyfunctional ligands with several sites forming the coordination bonds provides diversity in such complexes[2]. Several studies on copper complexes with en have been reported in past. A brief review of some of them is given below.

Bisethylenediaminecopper(II) nitrate has been prepared by Komiyama and Lingafelter[3] and its crystal structure determined to be distorted octahedral. Brown and Lingafelter[4] synthesized the complex $[Cu(en)_2](SCN)_2$ and determined its crystal structure to be octahedral. Inada *et al*.[5] have determined the structure of Cu(II) complex with en: $Cu(en)_3SO_4$in aqueous and neat en solutions by EXAFS and found it to be axially elongated octahedral with three en molecules. Fun *et al*.[6] have prepared the complex bis(ethylene-diamine) copper(II) bis(O,O′-diethyl dithiophosphate) and determined its crystal structure to be slightly distorted square planar.Wang and Yang[1] synthesized copper complexes of ethylenediamine, N-methylethylenediamine, N,N-dimethylethylenedia mine, N,N,N′-trimethylethylenediamine, and N,N,N′,N′-tetramethylethylenediamine and studied the complexes by pulsed-field ionization zero electron kinetic energy (ZEKE) and photoionization efficiency spectroscopies and second-order Moller-Plesset perturbation theory. The combination of the spectroscopic measurements and ab initio calculations has identified a hydrogen-bond-stabilized monodentate

*Corresponding author: E-mail: monicabairagi14@gmail.com

structure for the Cu-en complex and bidentate cyclic structures for the methyl-substituted derivatives. Sharma *et al*.,[7] have synthesized two Cu(II) complexes: $[Cu(en)_2(H_2O)_2](2\text{-phenoxybenzoate})_2\cdot H_2O$ and $[Cu(en)_2(H_2O)](diphenylacetate)_2\cdot 3H_2O$ and determined their structures by single crystal X-ray analysis. While, the first complex exhibits a distorted octahedral geometry with four nitrogen atoms of chelating en ligands and two oxygen atoms of water molecules coordinated to central Cu(II) ion, the second shows a square pyramidal geometry around Cu(II) with four nitrogen atoms of chelating en ligands and one oxygen atom of water molecule. The complex $[Cu(en)_2CrO_4]_n$ has been synthesized by Sukhikh *et al*.[8]. Single crystal X-ray diffraction analysis demonstrated that the synthesized complex was isostructural with $[Cu(en)_2SO_4]_n$ and has distorted octahedral structure. Four chiral Cu(II) complexes with terpene derivatives of en were synthesized by Gureva *et al*.[9] and their antibacterial, antifungal and antioxidant activities were studied. The crystal structure of one of the four complexes was determined and found to be trigonal–bipyramidal.

In the present investigation, X-ray absorption spectroscopy (XAS) at the Cu K-edge has been used to study the local and electronic structure of four copper complexes involving ethylenediamine (en) as primary ligand, viz: $Cu(en)_2Br_2.H_2O$ (**1**), $Cu(en)_2Cl_2.H_2O$ (**2**), $Cu(en)_2(ClO_4)_2$ (**3**) and $Cu(en)_2SO_4$ (**4**). The various studies done on these complexes have been discussed here in brief. Werner and Spruck[10] have isolated the ethylenediamine copper complexes **1, 2** and **4**. Complex **1** has been synthesized by Grossmann and Schuck[11] also. These authors merely prepared the complexes without further studying them. Mazzi[12] again prepared the complexes **1** and **2** and determined their crystallographic, optical, and structural properties. By electrolytic determination of copper, they confirmed that there is only one molecule of water in the two complexes, i.e., the formulae of the complexes **1** and **2** should have only $1H_2O$. Both the complexes have been reported to have distorted octahedral coordination around copper atom. Miskowski *et al*.[13] synthesized **1**, **2** and **3** complexes and studied their electronic, Raman, infrared and NMR spectra. Complex **1**has been synthesized again by Myznikov *et al*.[2] and characterized using X-ray diffraction analysis. It was found that the complex cation of **1** consists of Cu^{2+} ion coordinated with two en molecules, an H_2O molecule and Br^- anion in distorted octahedral geometry, as also reported by Mazzi[12]. However, the bond distances reported by Myznikov *et al*., are slightly different from those reported by Mazzi. The ESR and the optical absorption of complex **3** and seven other Cu(II) complexes of alkylated ethylenediamines have been investigated by Yokoi and Isobe[14] in order to estimate the character of the chemical bonding. Maxcy and Turnbull[15] prepared the complex**3** and reported its crystal structure to be axially distorted octahedral. Vakulka *et al*.[16] prepared the crystals of $[Cu^{II}(en)_2(H_2O)_2]$ $[Cu^{II}(OSO_3)_2(en)_2]\cdot 6H_2O$ and characterized them using single crystal X-ray diffraction. $[Cu^{II}(en)_2(H_2O)_2]^{2+}$ and $[Cu^{II}(OSO_3)_2(en)_2]^{2-}$ ions (complex **4**), were not found to be connected directly, but only via hydrogen bonding's. They have reported the structure of complex **4** to be distorted octahedral. Baldwin[17] synthesized complex **4** and studied its diffuse reflectance spectra and infrared spectra. This complex was also synthesized by Kajnakova *et al*.[18] and its crystal structure were determined to be distorted octahedral. Magnetic susceptibility and magnetization studies on this complex were also performed.

Though the crystal structures of the complexes **1**-**4** have been studied using X-ray crystallography, none of the complexes has been studied by X-ray absorption spectroscopy. It may be remarked here that the X-ray crystallography is undoubtedly the best method for determination of structure of a complex, but has an important constraint that the sample must be crystalline. For XAS, there is no such constraint and is an effective tool for investigating local structure and electronic nature of metal ions around the central absorbing atom in nearly all types of samples[19]. In the present work we have used powdered samples. Further, Levina *et al*.[20] have given reasons for using EXAFS even when structure has been studied by X-ray crystallography. Hence, it was considered worthwhile to study the local structures around Cu ion in the complexes **1**-**4** using extended X-ray absorption fine structure (EXAFS) and the electronic structure of Cu ions using X-ray absorption near edge structure (XANES). Also, XANES can provide valuable information about the oxidation state and the coordination geometry of the absorbing atom as well as the distortion caused by interaction of metal-ligand orbitals.[21]

The EXAFS of the complexes have been analyzed using their own available crystallographic data employing software *Athena* and *Artemis*. The XANES

spectra have been simulated for the Cu centre in the complexes using software *FEFF10* and compared with the experimental XANES spectra. Further, p-DOS and d-DOS have been calculated for the absorbing Cu metal center and correlated with the features and shape of the simulated XANES spectra as well as of the experimental spectra. The list of complexes **1-4** studied in the present work, with their codes and molecular formula are given in the Table 1.

It may be remarked here that the X-ray absorption spectra at the Cu K-edge of the four complexes have been studied earlier by the authors[22] using bent mica crystal 0.4m Cauchois type transmission spectrograph with sealed X-ray tube and recording the spectra on X-ray films. Also complexes **1**, **3** and **4** have been studied earlier by the authors[23], by recording the spectra on a dispersive type beamline and synchrotron radiation. The reason for undertaking the present investigation is that in these two earlier investigations, the spectra were not good in comparison to those recorded in the present investigation, using scanning type beamline and synchrotron radiation, and the EXAFS was not analyzed by fitting theoretical models and XANES was not analyzed by simulating the spectra and by calculating p- and d-DOS.

2 Experimental and Data Analysis

Complexes **1-3** have been prepared and characterized by following the methods described by Miskowski *et al.*[13] Complex **4** has been prepared and characterized by following the method described by Kajnakova *et al.*[18] The X-ray absorption spectroscopy (XAS) of the complexes have been recorded at the K-edge of copper on BL-9 scanning type EXAFS beamline at 2.5 GeV Indus-2 synchrotron source at Raja Ramanna Centre for Advanced Technology (RRCAT), Indore, India.[24] The main constituent of this beamline is a Double Crystal Monochromator (DCM), which has two Si (111) crystals carved out in a single block, the second crystal being sagittal cylinder. For recording XAS of complexes **1-4**, absorption screens were prepared in the form of pellets from the calculated amount of sample mixed with cellulose (binder). The spectrum of the Cu metal foil, required for energy calibration, is recorded simultaneous to the recording of the spectrum of the complexes. For calibration purpose, the first inflection point in the derivative spectrum of Cu metal foil was assigned the value of ~8979 eV.XAS of reference compounds Cu_2O, CuO have also been recorded for XANES fingerprinting purpose.

Table 1 — List of complexes with their codes and molecular formula

Code	Name	Molecular formula
1	$Cu(en)_2Br_2.H_2O$	$Cu(C_2H_8N_2)_2Br_2.H_2O$
2	$Cu(en)_2Cl_2.H_2O$	$Cu(C_2H_8N_2)_2Cl_2.H_2O$
3	$Cu(en)_2(ClO_4)_2$	$Cu(C_2H_8N_2)_2(ClO_4)_2$
4	$Cu(en)_2SO_4$	$Cu(C_2H_8N_2)_2\ SO_4$

Note: en=ethylenediamine

EXAFS data analysis was performed using the software packages *Athena* and *Artemis*.[25] The program *Athena* was first used to process the raw data to obtain normalized absorption coefficient μ(E) vs. energy E spectra, which are converted to χ(k) spectra and then Fourier transformed into R-space. The χ(k) vs. k spectra for the four complexes **1-4** are given in Fig. 1(a-d) and the Fourier transformed |χ(R)| vs. R spectra are given in both the Figs. 2 (a-d) and 3(a-d). Using program *Artemis*, theoretical models were generated using the available crystallographic data, which were fitted to the experimental data in k- space and R-space to determine the structural parameters including bond length (R), coordination number (N) and Debye-Waller factor, (σ^2). Ab-initio XANES calculations have been performed for the complexes by using computer code *FEFF10*[26], to obtain the simulated XANES spectra and the angular momentum projected electron density of states which are particularly helpful in interpretation of XANES.

3 Results and Discussions

3.1 EXAFS Analysis

The crystal structures of complexes **1** and **2** have been studied by Mazzi[12], of complex **3** by Maxcy and Turnbull[15] and of complex **4** by Kajnakova *et al.*[18] All the four complexes have distorted octahedral structure having four N atoms of two en ligands forming the square base with Cu atom at the center. In complexes **1** and **2**, Br/Cl atoms are at the axial position and the octahedral structure is completed by the O atom of the water molecule at another axial position. In complexes **3** and **4**, the octahedral structure is completed by the two O atoms of ClO_4 and SO_4 molecules respectively at the axial positions.

The analysis of the experimental EXAFS of the complexes has been done by generating the theoretical models and fitting them to the experimental data using software *Artemis*. Four theoretical models have been generated for the four complexes, using the available crystallographic data.

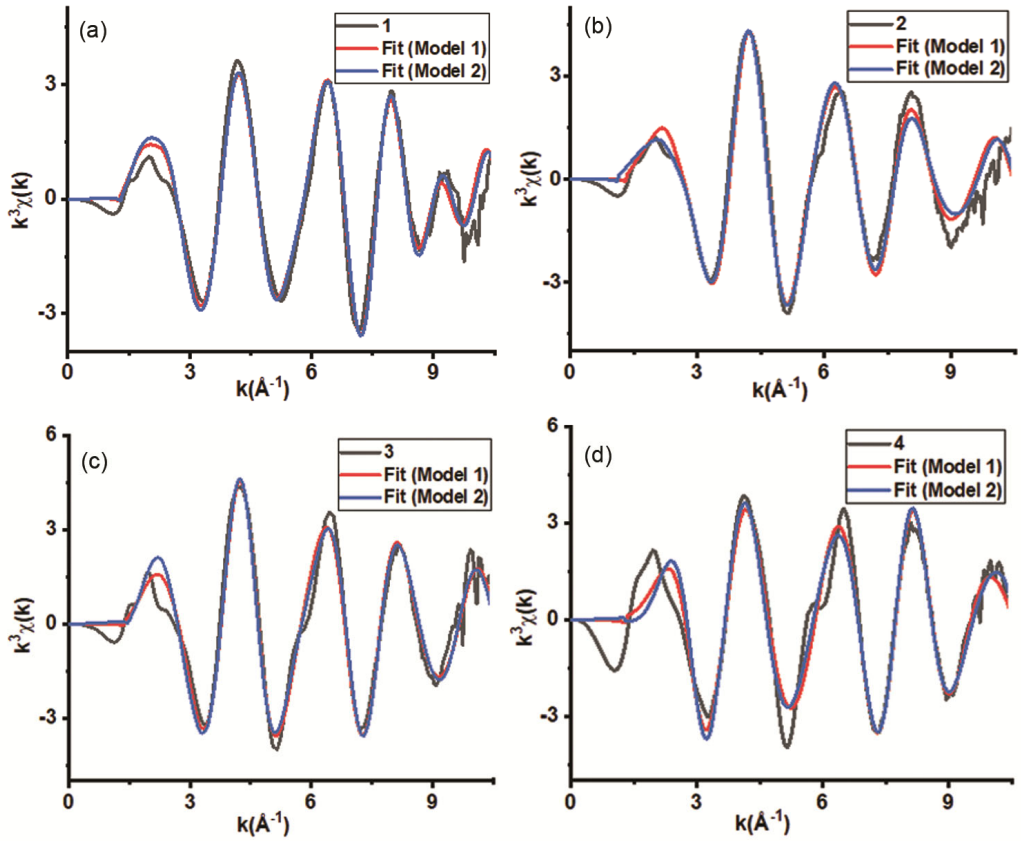

Fig. 1— Experimental k^3 weighted χ(k) vs. k spectra (black line) along with the theoretically fitted spectra by method A (red line) and by method B (blue line) (a) for **1,** (b) for **2,** (c) for **3,** and (d) for **4**

The CIF data for complexes **1** and **2** have been taken from Mazzi[12], of **3** from Maxcy and Turnbull[15] and of **4** from Kajnakova *et al*.[18] List of the first 10 scattering paths generated by *Artemis* for the four models are given in Table 2(a-d).In these tables, theR_{eff}(half-path length), N_{degen}(degeneracy) and amplitude are also given. For the analysis of EXAFS, the theoretical models have been fitted to the respective experimental data by two methods. In method A, the coordination number N has been varied and amplitude reduction factorS_0^2 has been fixed. In method B, N has been fixed and S_0^2 has been varied. The details of the analysis by the two methods are given below.

3.1.1 EXAFS Analysis by Method A (determining N)

In the four theoretical models, there are four atoms which are nearly at the same distance at equatorial positions. While performing the fitting of the theoretical model with the respective experimental data by method A, we have included only one path out of the paths for the four atoms, and guessed the coordination number (N) for the selected path. In complex **1**, first path, i.e., one of the four equatorial paths (having N_{degen}=1), and sixth and tenth paths, i.e., the two axial paths have been used. In complex **2**, first path (having N_{degen}=2), i.e., one of the three equatorial paths, and fourth and ninth paths, i.e., the two axial paths have been used. In the first path, the degeneracy has been changed from 2 to 1 in *Artemis*. In complex **3**, first path, i.e., one of the two equatorial paths (having N_{degen}=2), and third path, i.e., the axial path (N_{degen}=2) have been used. In the first path the degeneracy has been changed from 2 to 1 in *Artemis*. In complex **4**, first path, i.e., one of the two equatorial paths (having N_{degen}=2), and third and fourth paths, i.e., the two axial paths have been used. In the first path the degeneracy has been changed from 2 to 1 in *Artemis*. The coordination number (N) for the axial paths has been fixed as given in the model, because it is hard to accurately determine the coordination number (N) for the two distinct axial bonds given the limits of EXAFS analysis.[21]

For choosing the value of S_0^2, the following procedure has been adapted. The theoretical model for Cu metal has been first generated in *Artemis* and then

Table 2 — List of the first 10 scattering paths generated by *Artemis* along with their R_{eff} (half-path length), N_d (degeneracy) and amplitude

Path index	R_{eff} (Å)	N_d	amp	Scattering path	R_{eff} (Å)	N_d	amp	Scattering path
	(a) Complex **1**[12]				(b) Complex **2**[12]			
1	1.978	1	100	N2	1.988	2	100	N1
2	1.983	1	98.19	N3	1.990	1	49.89	N2
3	1.984	1	98.14	N4	1.993	1	49.72	N4
4	1.988	1	97.65	N1	2.686	1	24.28	O1
5	2.772	1	42.78	C2	2.801	1	21.32	C2
6	2.777	1	43.02	O1	2.806	1	21.22	C3
7	2.785	1	42.31	C4	2.809	1	21.16	C1
8	2.795	1	41.96	C1	2.822	1	20.96	C4
9	2.875	1	39.17	C3	3.000	1	25.52	Cl1
10	3.000	1	44.31	Br1	3.136	1	12.06	C2 N2
	(c) Complex **3**[15]				(d) Complex **4**[18]			
1	2.012	2	100	N2	2.015	2	100	N1
2	2.019	2	95.62	N1	2.020	2	99.49	N2
3	2.598	2	57.33	O3	2.360	1	37.39	O3
4	2.834	2	41.22	C2	2.470	1	33.64	O1
5	2.883	2	39.58	C1	2.484	2	16.97	H1
6	3.155	4	18.83	C2 N2	2.495	2	16.79	H2
7	3.202	4	18.26	C1 N1	2.717	8	11.88	H1 N1
8	3.407	4	6.99	N1 N2	2.718	4	6.03	H1 N2
9	3.465	4	6.09	N1 N2	2.821	2	41.61	C2
10	3.513	2	26.53	N3	2.858	2	40.36	C1

it is fitted to the experimental EXAFS spectra of the Cu metal foil, used as reference (standard), during the same experiments in which the spectra of the complexes were recorded. From this fitting, the value of S_0^2 has been found to be 0.95. This value of S_0^2 has been set for all the paths while fitting the theoretical model.

The other parameters used in the fitting were as follows. A single value of ΔE_0 has been defined for all the paths, but different values of ΔR have been defined for different paths. Debye-Waller factor (σ^2) values have been defined for each type of scattering path. The input parameter R_{bkg} was set to 1 Å. The range of the R-space was 1-3.2. The range of the k-space in which these fittings have been done are given in Table 3(a-d).

The experimental k^3 weighted $\chi(k)$ vs. k spectra along with theoretically fitted spectra are given in Fig. 1(a-d). The theoretically fitted spectra in R-space along with the contributions of the different paths used in the fitting are shown in Fig. 2(a-d). The local structure parameters around the absorbing Cu atom obtained as a result of the fitting are given in Table 3 (a-d). It can be seen that the bond distances obtained from EXAFS agree well with those reported by crystallography[12,15,18] (also given in the Table) for the octahedral geometry for all the four complexes. In this table the coordination number for the four equatorial atoms is found to be

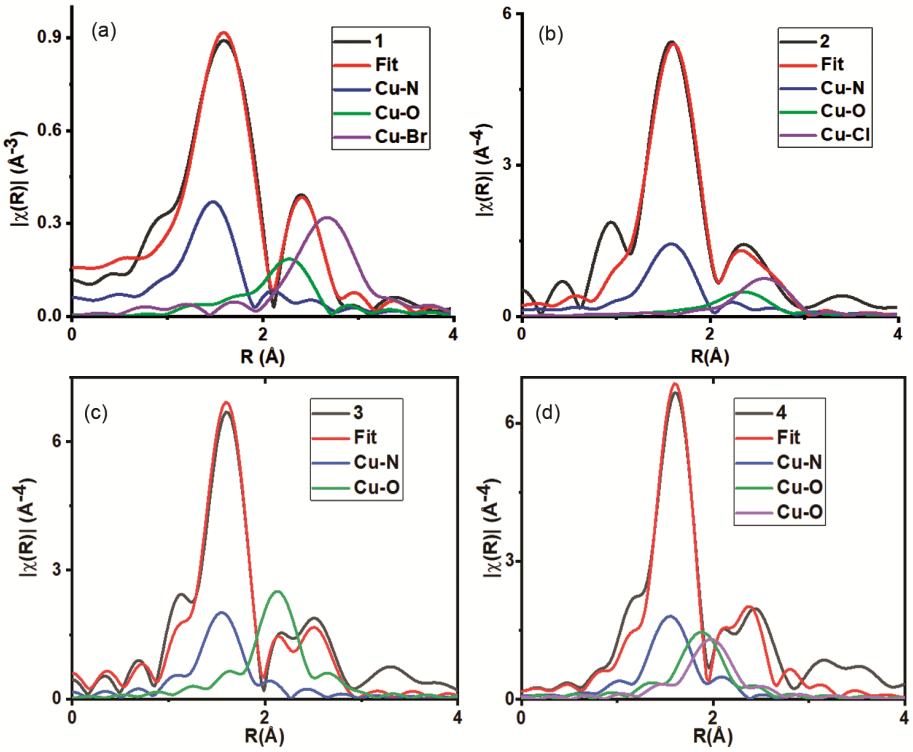

Fig. 2 — EXAFS fitting, by method A, in R-spacealong with contributions of the different paths, showing experimental curve (black line) and theoretical fit (red line). (a) for**1,** (b) for **2,** (c) for **3,** and (d) for 4

Table 3 — Structural parameters obtained from EXAFS fitting for complexes 1-4

N=coordination no., R=Bond distance, R c = crystallographic value, σ 2 = Debye-Waller factor, 'R factor'= Goodness of fit parameter, Error bars are given in parenthesis

Method A				Method B				Crystallographic value
(a) Complex 1: $Cu(en)_2Br_2.H_2O$								
S_0^2=0.95, ΔE_0=6.4(1.4) eV, '*R factor*'=0.00832, k-range=2.5-10.8				S_0^2=0.95(0.1), ΔE_0=6.6(1.4) eV, '*R factor*'=0.00800, k-range=2.5-10.8				
Atomic pairs	N	R (Å)	σ^2 x10^3 (Å^2)	Atomic pairs	N	R (Å)	σ^2 x10^3 (Å^2)	R_c[12] (Å)
Cu-N/O	3.9 (0.1)	2.03(0.01)	4.5(2.1)	Cu-N	1	2.02(0.01)	4.5(2.1)	1.988(N1),
				Cu-N	1	2.04(0.01)	4.5(2.1)	1.978(N2),
				Cu-N	1	2.04(0.01)	4.5(2.1)	1.983(N3),
				Cu-N	1	2.05(0.01)	4.5(2.1)	1.984(N4)
Cu-O	1	2.87(0.04)	8.4(2.4)	Cu-O	1	2.87(0.04)	8.4(2.4)	2.785
Cu-Br	1	2.79(0.01)	8.4(2.4)	Cu-Br	1	2.79(0.01)	8.4(2.4)	3.000
(b) Complex 2: $Cu(en)_2Cl_2.H_2O$								
S_0^2=0.95, ΔE_0=5.7(1.1) eV, '*R factor*'=0.00353, k-range=2.5-10.2				S_0^2=0.94(0.1), ΔE_0=6.5(1.5) eV, '*R factor*'=0.00358, k-range=2.5-10.2				
Atomic pairs	N	R (Å)	σ^2 x10^3 (Å^2)	Atomic pairs	N	R (Å)	σ^2 x10^3 (Å^2)	R_c[12](Å)
Cu-N/O	3.8(0.2)	2.03(0.01)	7.3(1.5)	Cu-N	2	2.03(0.01)	7.7(1.5)	1.988(N1), 1.988(N1)
				Cu-N	1	2.04(0.01)	7.7(1.5)	1.990(N2),
				Cu-N	1	2.04(0.01)	7.7(1.5)	1.993(N3)
Cu-O	1	2.81(0.03)	11.9(3.4)	Cu-O	1	2.81(0.02)	13.4(3.4)	2.686
Cu-Cl	1	3.01(0.04)	11.9(3.4)	Cu-Cl	1	3.01(0.03)	13.4(3.4)	3.000
(c) Complex 3: $Cu(en)_2(ClO_4)_2$								
S_0^2=0.95, ΔE_0=5.0(1.6) eV, '*R factor*'=0.00664, k-range=2.5-11.5				S_0^2=0.94(0.1), ΔE_0=5.2(2.2) eV, '*R factor*'=0.00138, k-range=2.5-11.5				
Atomic pairs	N	R (Å)	σ^2 x10^3 (Å^2)	Atomic pairs	N	R (Å)	σ^2 x10^3 (Å^2)	R_c[15](Å)
Cu-N/O	3.7(0.3)	2.00 (0.01)	4.9 (1.5)	Cu-N	2	1.98 (0.01)	5.1 (1.6)	2.012(N4), 2.012(N4),
				Cu-N	2	2.02 (0.01)	5.1 (1.6)	2.019(N1), 2.019(N1)
Cu-O3	2	2.76 (0.06)	7.8(3.8)	Cu-O3	2	2.76 (0.1)	15.6(6.8)	2.598, 2.598
(d) Complex 4: $Cu(en)_2SO_4$								
S_0^2=0.95, ΔE_0=4.6(2.0) eV, '*R factor*'=0.00157, k-range=2.5-12.1				S_0^2=0.96(0.2), ΔE_0=4.3(2.8) eV, '*R factor*'=0.00189, k-range=2.5-12.1				
Atomic pairs	N	R (Å)	σ^2 x10^3(Å^2)	Atomic pairs	N	R (Å)	σ^2 x10^3 (Å^2)	R_c[18] (Å)
Cu-N/O	3.9(0.1)	2.01(0.01)	4.7(1.8)	Cu-N	2	2.02(0.01)	5.3(2.3)	2.015(N1), 2.015(N1),
				Cu-N	2	2.02(0.01)	5.3(2.3)	2.020(N2), 2.020(N2)
Cu-O3	1	2.37(0.03)	12.5(9.1)	Cu-O3	1	2.36(0.03)	8.8(4.2)	2.360
Cu-O4	1	2.48(0.03)	12.5(9.1)	Cu-O4	1	2.47(0.03)	8.8(4.2)	2.470

3.9(0.1), 3.8(0.2), 3.7(0.3) and 3.9(0.1) in the four complexes **1-4,** respectively. The coordination number can thus be taken as 4, i.e., there are four equatorial atoms around the absorbing Cu atom. In EXAFS analysis it is difficult to distinguish between O and N atoms, hence we have written O/N in the Table 3(a-d). When ethylenediamine complex with Cu is formed, two N atoms of each of the two ethylenediamine form four Cu-N bonds. Hence, while depicting the geometry of the complexes around the Cu atom in Fig. 4(a-d), we have preferred to write N instead of O/N.

3.1.2 EXAFS Analysis by Method B (Determining S_0^2)

As mentioned in Section 3.1, an alternate method of analysis of EXAFS, designated as method B, has also been used for fitting the theoretical model to the experimental EXAFS data. In this method the value of coordination number N is fixed, i.e., as given in the list of paths given in Table 2 (a-d) and the amplitude reduction factor S_0^2 is varied. The parameters used in the fitting, viz., ΔE_0, ΔR, $\sigma^2 R_{bkg}$ and range of the R-space were the same as used in method A. The range of the k-space in which these fittings have been done are given in Table 3 (a-d).

The paths included in the fittings were as follows: In complex **1**, first four paths, i.e., equatorial paths, and sixth and tenth paths, i.e., the two axial paths, have been used. In complex **2**, the first path (N_{degen}=2) and second and third paths, i.e., equatorial paths and

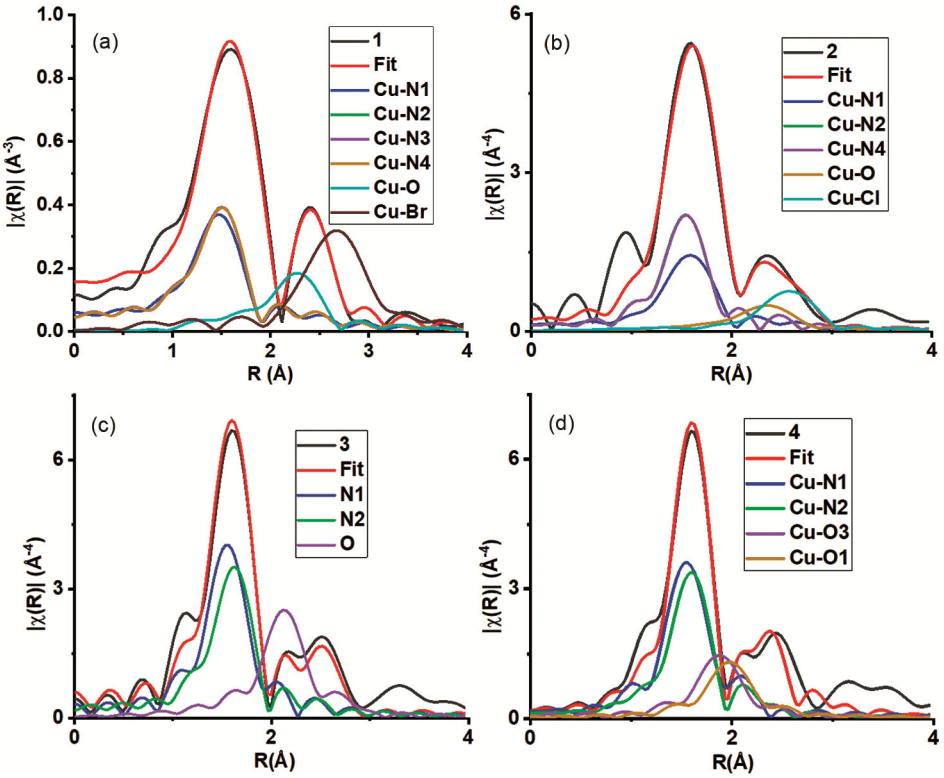

Fig. 3 — EXAFS fitting, by method B, in R-spacealong with contributions of the different paths, showing experimental curve (black line) and theoretical fit (red line). (a) for**1,** (b) for **2,** (c) for **3** and (d) for **4**

fourth and ninth paths, i.e., the two axial paths, have been used. In complex **3**, first two paths (each having N_{degen}=2), i.e., equatorial paths, and third path, i.e., the axial path (N_{degen}=2), have been used. In complex **4**, first two paths (each having N_{degen}=2), i.e., equatorial paths, and third and fourth paths, i.e., the two axial paths, have been used. The experimental k^3 weighted χ(k) vs. k spectra along with theoretically fitted spectra by method B are given in the same Fig. 1(a-d), in which the fittings by method 1 are also given. The theoretically fitted spectra in R-space along with the contributions of the different paths used in the fitting are shown in Fig. 3(a-d).The local structure parameters around the absorbing Cu atom obtained as a result of fittings, by method B, are given in Table 3(a-d). The geometries of complexes **1-4** around the Cu atom are the same as shown in Fig. 4 (a-d), in which the bond lengths obtained by this method are given in different color. The bond distances obtained from the two methods given in Table 3 (a-d) and shown in Fig. 4(a-d) are nearly the same. However, method A appears to be better because in this method N is determined and thus the structure is also determined

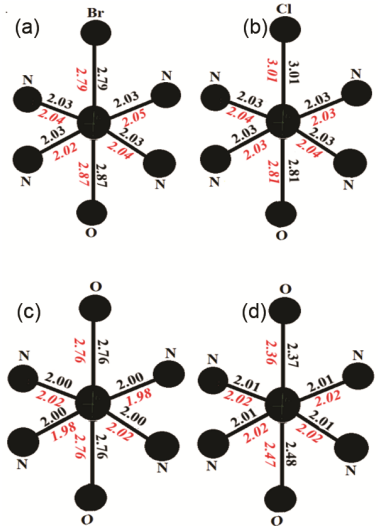

Fig. 4— Distorted octahedral coordination geometry for Cu in (a) for **1,** (b) for **2,** (c) for **3** and (d) for **4**. The bond lengths shown (in Å) are determined from EXAFS analysis by method A (black) and method B (red)

3.2 XANES Interpretation

Normalized Cu K-edge XANES spectra for the complexes **1-4** are shown in Fig. 5 (a). The reference spectra of Cu metal, CuO, Cu_2O showing characteristic

XANES features for different oxidation states of Cu are also given in this figure for comparison.The K-edge is seen split into two portions: K_1 and K_2 with a shoulder, marked as S, separating the two portions. The pre-edge peak, marked as P, is very weak. The white line W has been found to have a broadened two peak like structure. The peaks have been marked by two arrows in the figure.

3.2.1 Chemical Shift

From Fig. 5(a), it can be seen that, as expected, the Cu K-edge in the compounds and complexes is found to be shifted to the higher energy side as compared to that of Cu metal. The edge energy can be measured easily and accurately from the derivative XANES spectra given in Fig. 5 (b). The two peaks K_1 and K_2 in the derivative spectra correspond to the two portions K_1 and K_2 of the Cu K-edge. As the peak K_1 in the derivative spectra corresponds to the inflection point of the K_1 edge, its energy E_{K1} is taken as the Cu K-edge energy and can be accurately measured as the energy of the K_1 peak in the derivative spectra. The shift in edge energy (E_{K1}) of the compounds and complexes with respect to that of Cu metal (8979 eV), known as chemical shift, is collected in Table 4. The chemical shift is found to be 4.9, 5.0, 4.9, 6.2 eV for complexes **1**-**4** respectively. In the standard compounds Cu_2O and CuO, the shift is found to be 1.2 eV and 5.9 eV respectively. On comparing these shifts, it can be seen that the complexes **1**-**4** show shifts of the order of that obtained in CuO. Since, the chemical shift has been recognized as a good indicator of the oxidation state of the absorbing atom, it can be concluded that in the complexes **1**-**4**,Cu is in +2 oxidation state.

3.2.2 Ab-initio XANES Calculations

Ab-initio XANES calculations have been performed using the software *FEFF10*[26] to obtain simulated XANES spectra as well as p and d-DOS for the complexes **1**-**4**. This program requires feff.inp file for calculations. The feff file which has been generated in *Artemis* for a complex, utilizing the available crystal structure data[12,15,18] contain the distances of the atoms surrounding Cu central metal ion as determined by crystallography. The feff file is imported in *FEFF10* as feff.inp file. Before importing the file, the crystallographic distances for the first coordinate sphere in the file are replaced by the

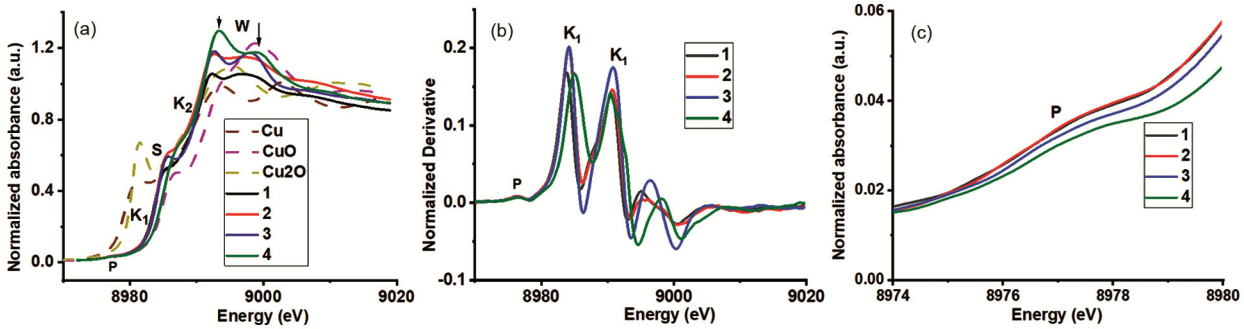

Fig. 5 — (a) Normalized Cu K-edge XANES spectra of complexes **1**-**4.** The spectra of Cu metal, CuO, Cu_2O are also included for comparison. The pre-edge peak is marked as P. White line is marked as W and has a broadened two peak like structure, the two peaks being marked by two arrows. The K-edge is seen split into two portions: K_1 and K_2 with a shoulder S in between. (b) Derivative XANES spectra of complexes **1**-**4**, and (c) Pre-edge peak P, shown enlarged

Table 4 — XANES experimental data and analysis data

Complex	Experimental data				Theoretical data	
	E_{K1} (eV)	E_{K2} (eV)	Chemi-cal shift* (eV)	Separation of peaks K_1 and K_2 in derivative of experimental spectra (E_{K2}- E_{K1}) (eV)	Separation of peaks K_1 and K_2 in derivative of simulated spectra (E_{K2}- E_{K1}) (eV)	Separation of peaks A and B in p-DOS (eV)
1	8983.9	8990.5	4.9	6.6	6.9	8
2	8984.0	8990.8	5.0	6.8	7	8
3	8983.9	8990.5	4.9	6.6	7.2	8.4
4	8985.2	8991.3	6.2	5.8	6.6	7

Notes: *Chemical shift= E_{K1}(Compound)-E_{K1}(Cu metal)
E_{k1}(Cu metal) = 8979 eV
Chemical shifts for Cu_2O is 1.2 eV, CuO is 5.9 eV

distances determined from EXAFS analysis, so that proper results may be obtained in XANES calculations. In the calculations, Hedin-Lundqvist potential was chosen and the cards called 'XANES', 'Exchange', 'SCF' (Self-Consistent Field) and 'FMS' (Full Multiple Scattering) were used. SCF parameters were kept as follows: nscmt = 100, lfms1 = 0, rfms1 = 4, ca = 0.2, nmix = 1. The XANES parameters were as follows: vixan = 0.1, xkstep = 0.07, xkmax = 4 and cluster size= 8 Å. For density of states calculations, the 'LDOS' card with an energy range of −20 to 40 eV has been used. The simulated spectra of complexes **1-4** are given in Fig. 6(a-d). In these figures the experimental XANES spectra are alsogiven, so that the features and shape of the simulated XANES spectra can be compared with the experimentally measured spectra. For correlating both the experimental and simulated spectra with the theoretical p-DOS, the latter is also included in Fig. 6

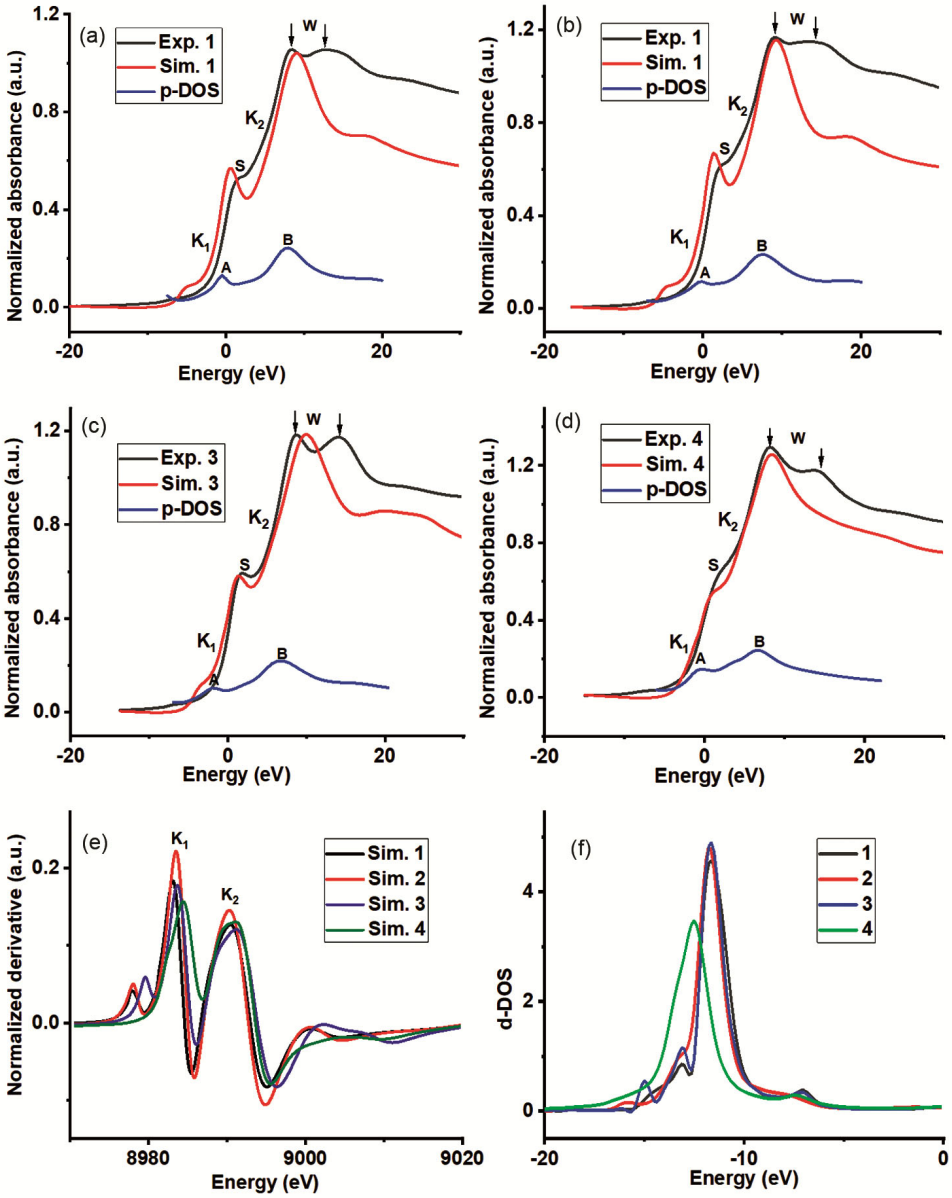

Fig. 6— Simulated XANES spectra (Sim.), experimental XANES spectra (Exp.) and p-DOS (a) for **1,** (b) for **2,** (c) for **3** and (d) for **4**. The simulated and experimental spectra have been aligned by *Athena*. The K-edge is seen split into two portions: K_1 and K_2 with a shoulder S in between in both the simulated and experimental spectra. The two peaks in the p-DOS, marked as A and B, correspond to K_1 and K_2 respectively. White line is marked as W, (e) Derivative of simulated XANES spectra for complexes **1-4**, and (f) Theoretical d-DOS calculated by using *FEFF10* for complexes **1-4**

(a-d). The theoretically calculated p- and d-DOS have been further used for discussion in the following sections.

3.2.3 Derivative Spectra

The Cu K-edge arises due to electric dipole-allowed 1s→4p transition and is found to be split into two edges K_1 and K_2 by a shoulder in all the four complexes (fig. 5(b)), the two edges being due to 1s→$4p_{xy}$ and 1s→$4p_z$ transitions respectively.[21,27] The two edges give rise to two peaks, which are also marked as K_1 and K_2, in the derivative spectra. The energy separation between the two edges K_1 and K_2 has been determined from the difference of energies of the two peaks K_1 and K_2 in the derivative spectra and is given in Table 4. It has been reported that the XANES features observed in the K absorption spectra of the complexes are indicative of their coordination geometries.[28-30] While, the K_2 edge is said to reflect the axial geometry of the metal clusters, the K_1 edge is said to reflect the distortion in the Cu cluster.[31] Further, the energy separation between the K_1 and K_2 edges, as determined from separation between two peaks K_1 and K_2 in the derivative spectra, is expected to give an estimate of the destabilization of the $4p_z$ metal orbital. Since the $4p_z$ destabilization can be correlated to the axial (z axis) bond length, hence the energy separation between peaks K_1 and K_2 should depend on the axial bond length. We have tried to plot the energy separation of peaks K_1 and K_2 in derivative of experimental spectra, as given in Table 4, with the average of the two axial bond lengths given in Table 3. The plot is given in Fig. 7. It can be seen from this plot that the energy separation of peaks K_1 and K_2 in derivative spectra usually increase with the increase in axial bond lengths.

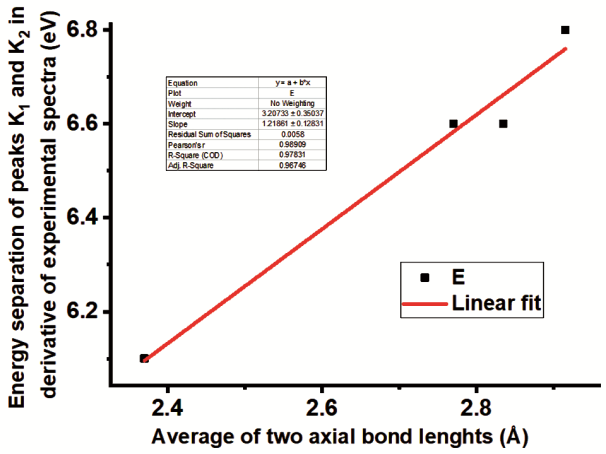

Fig.7 — Plot showing the correlation of the energy separation of peaks K_1 and K_2 in derivative of experimental spectra with the average of the two axial bond lengths

3.2.4 Correlation with the Splitting of the Edge with p-DOS

We have attempted to explain the splitting of the K-edge on the basis of the simulated XANES spectra (Fig. 6(e)) and the theoretically calculated p-DOS (Fig. 6(a-d)). In Table 4 are given the energy separation of peaks K_1 and K_2 in derivative of experimental spectra, energy separation of peaks K_1 and K_2 in derivative of simulated spectra and energy separation of peaks A and B in theoretically calculated p-DOS. The range of energy separation of peaks K_1 and K_2 in derivative of experimental spectra of the complexes is 5.8-6.8 eV, in the derivative of simulated spectra 6.6-7.2 eV and in p-DOS 7-8.4 eV. Thus, satisfactory agreement is found between the values of experimental derivative spectra and the simulated derivative spectra showing that experimental spectra of the complexes are well reproduced in the simulated spectra. Also, the range of separation of the two humps in the p-DOS for the four complexes is nearly the same as the range of separation between the experimental K_1 and K_2 edges. Hence, the two humps A and B in the p-DOS can thus be correlated with the two edges K_1 and K_2. The splitting of the K-edge into K_1 and K_2 edges in the complexes can thus be understood on the basis of density of 4p states.

3.2.5 Fitting of Pre-edge Peak withPseudo-Voigt Function

In the XANES spectra of the complexes **1-4** (Fig. 5(a)), the pre-edge peak P is seen as a weak feature. It is seen with some clarity in Fig. 5(c), which is a blown-up figure of the relevant portion of Fig. 5(a).Further, it is clearly observed in the derivative XANES spectra given in Fig. 5(b). The peak in Fig. 5(a) has been analyzed using the module available in software *Larch*.[32] Firstly, the peak is separated by subtracting the background from the experimental data (Fig. 5(a)). The separated peak is fitted by Pseudo-Voigt function. The separated peak and the fitting have been shown in Fig. 8(a-d) for complexes **1-4** respectively. The values of height, area (amplitude), FWHM, and centroid of the pre-edge peak, obtained from the fitting, are given in Table 5.The centroid of the peak is found in the energy range 8977.2 to 8977.4 eV. The occurrence of the pre-edge peak has been correlated with d-density of states in the following section.

3.2.6 Correlation of Pre-edge Peak with d-DOS

The pre-edge peak arises due to1s→3d quadrupole transition. The intensity of a transition is proportional

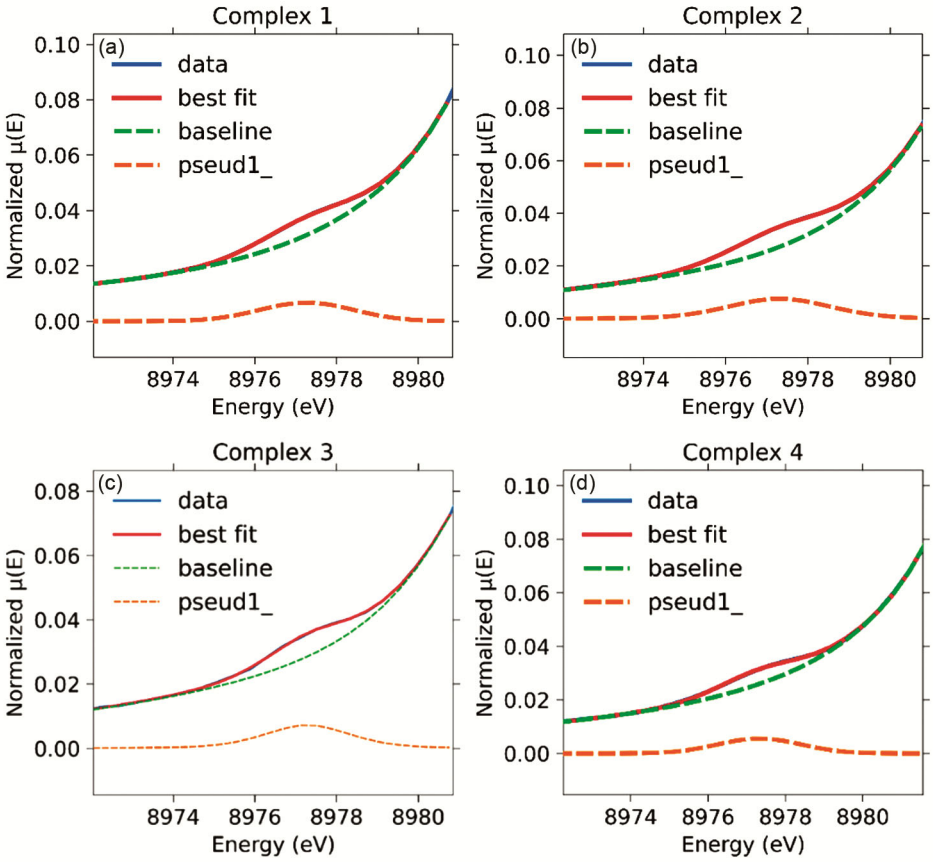

Fig. 8 — Analysis of pre-edge peak using the module available in software *Larch* and fitting it by Pseudo-Voigt function

Table 5 — Pre-edge peak experimental data and analysis data

Complex	Experimental data of pre-edge peak						Theoretical d-DOS data		
	E (Centr-oid) (eV)	E(com-plex)*-E(cent-roid)	Height (arb. units) $\times 10^{-3}$	FWHM (arb. units)	Area (arb. units) $\times 10^{-3}$	χ_ν^2 ** $\times 10^{-9}$	Position of maxima (eV)	Height of maxima (arb. units)	Area of curve (arb. units)
1	8977.2	8	7.1	2.68	21	3.9	11.5	4.5	8.6
2	8977.3	8.2	7.7	2.91	26	4.3	11.8	4.8	10.5
3	8977.3	7.9	7.2	2.46	22	4.2	11.5	4.7	8.6
4	8977.4	9.7	6.3	2.71	19	1.1	12.5	3.5	7.9

Notes: *E(complex) has been determined as a energy corresponding to normalized μx=0.5[19,38]
**χ_ν^2 is the parameter for fitting the Pseudo-Voigt function to the pre-edge peak.

to the product of the probability of transition and the density of vacant state.[33,34] The transition probability of the quadrupole transition is very low, (of the order of <1/100) in comparison to the dipole transition 1s→4p which gives rise to the edge.[34-37] Hence, we have tried to correlate the occurrence of the peak to the 3d-density of states, which have been theoretically computed for the complexes **1-4** and are shown in fig. 6(f). The theoretical d-DOS peaks at 11.5-12.5 eV below the position of the K-edge in the complexes and this position has been compared with the position of the pre-edge peak in the experimental spectra. For this purpose, we have first determined the energy of the Cu K-edge in the experimental spectra of the complexes at μx=0.5 position.[19,38] The position of centroid of the pre-edge peak in the experimental spectra (Fig. 8(a-d)) has been then found to be in the range 7.9-9.7 eV with respect to this Cu K-edge energy. This range is slightly less than the range of the position of the peak of the theoretical d-DOS. A reason for the difference in the theoretical and experimental positions could be that in the *FEFF10*

calculations, the edge energy of Cu K-edge in the metal, i.e., 8979 eV is used as input instead of the energy of the edge in the complex. In any case, the position of pre-edge peak in the experimental spectra can be taken to be corresponding to the position of the peak in the theoretical 3d-density of states. Nevertheless, the significant value of the density of 3d states, shown in Fig. 6(f), is an important reason for the occurrence of pre-edge peak, though the quadrupole transition responsible for it has low probability.

3.2.7 White Line

Just after the rising portion of the Cu K-edge (fig. 6(a-d)), the white line W has been observed as a broadened two peak like structure. The two peaks have been marked by two arrows in the figures. The separation of the two peaks has been found to be 4.5, 4.1, 5.7 and 5.7 eV in the complexes **1-4,** respectively. The white line arises due to the transitions from Cu 1s orbital to mainly 4p molecular orbitals.[39] In the same figures the simulated XANES spectra obtained from *FEFF10* calculations are also given, in which the white line is observed as a single peak and the two-peak structure of the white line is not seen. Regarding such difference in the experimental and the simulated XANES spectra, Chaboy*et al*.[40] have argued that single-channel multiple-scattering XANES calculations, taking the final state electronic configuration of Cu (II) as $3d^9$, are unable to reproduce the two-peak feature of white line in the simulated spectra. Hence, in their calculations for a tetramine copper(II) complex, they included the contributions of both of the electronic configurations $3d^9$ and $3d^{10}L$ in the final state. The relative weights were fixed as 68% and 32% respectively for $3d^{10}$ and $3d^9L$ electronic configurations. Good agreement was obtained between the simulated and experimental two peak like structure of white line. The calculated binding energies for the $3d^{10}$ and $3d^9L$ configurations were found to differ by 6.37 eV, which was very close to the experimental separation of the two peaks in the white line (5.98 eV). In the present case, the experimental separation is 4.1-5.7 eV in complexes **1-4**. Hence, the two peak like structure of the white line in complexes **1-4** can be attributed to the contribution of the two electronic configurations $3d^9$ and $3d^{10}L$ in the final state during the photo absorption process.

4 Conclusion

XAFS at the Cu K-edge in copper ethylenediamine mixed ligand complexes **1-4** have been investigated using synchrotron radiation. For the analysis of EXAFS, theoretical models have been generated for each complex using their available crystal structure data. The theoretical models have been fitted to the respective experimental data by two methods. In the first method A, the coordination number N has been varied and amplitude reduction factorS_0^2 has been fixed. In the second method B, N has been fixed and S_0^2 has been varied. From this analysis, the coordination geometry around the absorbing Cu center has been found to be distorted octahedral in all the four complexes, as also reported by crystallography. The four N atoms form the square base with Cu atom at the center in all the four complexes. In complexes **1** and **2**, Br/Cl atoms are at the axial position and the octahedral structure is completed by the O atom at another axial position. In complexes **3** and **4**, the octahedral structure is completed by the two O atoms at the axial positions. The geometries of the complexes around the Cu atom have been depicted in which the bond lengths shown (in Å) have been determined from EXAFS analysis by the two methods. The bond lengths obtained by the two methods are nearly the same and compare well with the crystallographic bond lengths.

Ab-initio XANES calculations have been performed to obtain simulated XANES spectra as well as p- and d-DOS for the absorbing Cu metal center. The simulated spectra show main edge features similar to those present in the experimental spectra. The Cu K-edge is found to be split into two edges K_1 and K_2 in all the four complexes. The two edges give rise to two peaks in the derivative spectra, which are also marked as K_1 and K_2. We have attempted to explain the splitting of the K-edge on the basis of the simulated XANES spectra and the theoretically calculated p-DOS.Satisfactory agreement has been found between the range of energy separation of peaks K_1 and K_2 in the derivative experimental spectra and the derivative simulated spectra, showing that the experimental spectra of the complexes are well reproduced in the simulated spectra. The range of energy separation of the two humps in the p-DOS is also nearly the same as the range of energy separation between the experimental K_1 and K_2 edges, indicating correlation between the two humps A and B in the p-DOS with the two edges K_1 and K_2 in the experimental spectra. The splitting of the K-edge into K_1 and K_2 edges in the complexes can thus be understood on the basis of density of 4p states.

In the XANES spectra of the four complexes, the pre-edge peak has been observed as a weak feature. After removing the background, the peak has been fitted by Pseudo-Voigt function and the values of height, area (amplitude), FWHM and centroid of the peak have been obtained. The peak arises due to 1s→3d quadrupole transition. The intensity of a transition is proportional to both the density of states and the transition probability. The quadrupole transition has very low transition probability and hence, the significant value of the theoretically calculated density of d states can be taken as an important reason for the occurrence of the pre-edge peak. The white line has been observed as two peak structures in the complexes due to the contribution of the two electronic configurations $3d^9$ and $3d^{10}L$ in the final state.

Acknowledgements

V.K. Hinge and M. Bairagi would like to thank the University Grant Commission-Department of Atomic Energy-Consortium for Scientific Research, Indore, India, for the research project grant No. CSR-IC-ISUM-24/CRS-307/2019-20/1359. Thanks are due to Dr. J. Prasad and K. Shrivastava for the samples and Dr. Abhijeet Gaur, for help throughout the investigation.

References

1 Wang X & Yang D S, *J Phys Chem A,* 110 (24) (2006) 7568.
2 Myznikova L V, Fisher A I, Dmitrieva U N, Artamonova T V &Zevatski Y E, *Russ J Gen Chem,* 88 (3) (2018) 495.
3 Komiyama Y & Lingafelter E C,*Acta Cryst*, 17 (1964) 1145.
4 Brown B W&Lingafelter E C, *ActaCryst,*17 (1964) 254.
5 Inada Y, Ozutsumi K, Funahashi S, Soyama S, Kawashima T & Tanaka M, *Inorg Chem* 32 (14) (1993) 3010.
6 Fun H K, Hao Q, Wu J, Yang X, Lu L, Wang X, Chantrapromma S, Razaka I A & Usman A, *ActaCryst,* C58 (2002) m87-m88.
7 Sharma R P, Saini A, Kumar S, Kumar J, Venugopalan P, Gondhil V S, Chibber S &Aree T, *Polyhedron,*123 (2017) 430.
8 Sukhikh A S, Khranenko S P &Gromilov S A, *J StructChem,* 59 (2018) 395.
9 Gureva Y A, Zalevskaya O A, Shevchenko O G, Slepukhin P A, Makarov V A &Kuchin A V, *RSC Adv,* 12 (15) (2022) 8841.
10 Werner A, Spruck W, Megerle W & Pastor J, *Z anorgChem,* 21 (1) (1899) 201.
11 Grossmann H &Schck B, *Z anorgChem,* 50 (1) (1906) 1.
12 Mazzi F, *R D Soc Miner, ltal*, 9 (1953) 148.
13 Miskowski V M, Thich J A, Solomon R &Schugar H J, *J Am ChemSoc,* 98 (26) (1976) 8344.
14 Yokoi H &Isob T, *Bull ChemSocJpn,* 42 (8) (1969) 2187.
15 Maxcy K R & Turnbull M M, *ActaCryst.* C55 (1999) 1986.
16 Vakulka A, Goreshnik E, Jagodic M, Jaglicic Z &Trontelj Z, *J MolStruct,* 1210 (2020) 128002.
17 Baldwin M E, *Spectrochim A,* 19 (1) (1963) 315.
18 Kajnakova M, Orendacova A, Orendac M &Feher A, *Acta Phys Pol A,* 113 (1) (2008) 50.
19 Calvin S, CRC Press, Boca Raton, Florida, USA (2013).
20 Levina A, Armstrong R S & Lay P A, *CoordChem Rev,* 249 (2005) 141-160
21 Hinge V K, Bairagi M, Yadav N, Joshi S K, Shrivastava B D, Jha S N, Bhattacharya D & Gaur A, *X-Ray Spectrom,* 53 (1) (2023) 60.
22 Hinge V K, Joshi S K, Shrivastava B D, Prasad J & Srivastava K, *J Phys ConfSer,* 365 (2012) 012029.
23 Dwivedi S, Joshi S K, Hinge V K, Shrivastava B D, Prasad J & Srivastava K, *J Phys Conf. Ser,* 534 (2014) 012006.
24 Gaur A, Dar D Ah, Shrivastava B D, Prasad J, Srivastava K, Jha S N& Bhattacharyya D, *Indian J Phys,* 89 (5) (2015) 453.
25 Ravel B & Newville M, *J Synchrotron Radiat,* 2 (4) (2005) 537.
26 Kas J J, Vila F D, Rehr J J, Pemmaraju C D & Tan T S, *J Synchrotron Radiat,* 28 (6) (2021) 1801.
27 Gaur A, Shrivastava B D, Srivastava K & Prasad J, *X-ray Spectrom,* 43 (4) (2014) 238.
28 Gaur A, Klysubun W, Nair N N, Shrivastava B D, Prasad J & Srivastava K, *J MolStruc,* 1118 (2016) 212.
29 Hinge V K, Bairagi M, Yadav N, Shrivastava B D, Jha S N, Bhattacharya D & Gaur A, *J MolStruc,* 1289 (2023) 135909.
30 Bairagi M, Hinge V K, Yadav N, Shrivastava B D, Jha S N, Bhattacharya D & Gaur A, *Radiat Phys Chem,* 218 (2024) 111609.
31 Dupont L, Guillon E, Bouanda J, Dumonceau J &Aplincourt M, *Environ SciTechnol,* 36 (23) (2002) 5062.
32 Newville M, *J Phys: ConfSer,* 430 (2013) 012007.
33 Sarmaha N, Sharma D, Mehta B K, Shrivastava B D, Das B K, Zimina A, Gaur A, *J. Mol. Struc.* 1263 (2022) 133125.
34 Blokhin M A, Second, Revised Edition, United States Atomic Energy Commission, Office of Technical Information, Germantown, Maryland, USA, 1961; page 285.
35 Bair R A & Goddard W A, *Phys Rev* B, 22 (6) (1980) 2767.
36 Agarwal B K, Springer-Verlag,Berlin,Heidelberg, Germany, 1998, 92.
37 Scofield J H, *Atom Data NuclData Tables*, 14 (2) (1974) 121.
38 Lamberti C, Bordiga S, Bonino F, Prestipino C, Berlier G, Capello L, D'Acapito F, Llabre´s i Xamena F X, and Zecchina A, *Phys ChemChem Phys,* 5(20) (2003) 4502.
39 Adak S, Hartl M, Daemen L, Fohtung E &Nakotte H, *J Electron SpectrosRelat Phenom,* 214 (2017) 8.
40 Chaboy J, Munoz-Paez A, Carrera F, Merkling P & Marcos E S, *Phys Rev B,* 71 (13) (2005) 134208.